ON INSTABILITIES AND TRANSITION IN LAMINAR SEPARATION BUBBLES

Ulrich Rist
Institut für Aerodynamik & Gasdynamik, Universität Stuttgart
D-70550 Stuttgart, Germany

Abstract

During the past several years we have performed a considerable amount of investigations of basic instability mechanisms in various laminar separation bubbles. Because of the high sensitivity of the flow with respect to intrusive measurement techniques and the difficulties of computing the flow field via boundary-layer equations or RANS our research relies primarily on direct numerical simulations (DNS) based on the complete Navier-Stokes equations, backed by linear stability theory, wind tunnel and (non-intrusive) water channel experiments. Using LDA and PIV it is now possible to measure unsteady flow quantities without influencing the flow. The investigations concentrate on different instability mechanisms and their possible contributions to laminar-turbulent transition in laminar separation bubbles. In the present contribution we shall present an overview on this research.

List of Symbols

A_v	amplitude of wall-normal forcing at disturbance strip
c_r	phase speed of disturbances
f	nondimensional circular frequency $2\pi f[Hz]\, L/U_\infty$
H_{12}	base-flow shape parameter
h_R	height of recirculation zone
L	reference length
Re	Reynolds number $U_\infty L/\nu$
Re^*	Reynolds number $U_\infty \delta^*/\nu$
u	downstream velocity component
U_∞	free-stream reference velocity
u_e	mean velocity at y_e
u'_{max}	wall-normal maximum of u disturbance
U_p	inviscid (potential) free-stream velocity
U_R	maximum of reverse-flow velocity
v	wall-normal velocity component
x	downstream coordinate
y	wall-normal coordinate
y_e	wall distance of the free-stream boundary of the integration domain
z	spanwise coordinate
α_i	spatial amplification rate
δ^*	displacement thickness
γ	spanwise wave number
λ_z	spanwise wave length
ν	kinematic viscosity
ω_i	temporal amplification rate
$\omega_{0,i}$	temporal amplification rate of modes with zero group velocity
ψ	obliqueness angle relative to the free-stream direction

Introduction

Laminar-turbulent transition is a key area of aerospace aerodynamics research because of its influence on fuel consumption via the drag. Despite many years of research on the fundamental mechanisms of the transition process in many generic configurations relevant for aircrafts, as well as other applications, there are situations which are less well understood and hence much more difficult to predict than certain ‘standard’ cases, as e.g. zero-pressure gradient flat-plate boundary-layer transition. Laminar separation bubbles are a typical example for such a more involved case.

When an adverse streamwise pressure gradient causes a laminar boundary layer to separate, the

flow is subject to increased instability with respect to small-amplitude disturbances present in the flow. Transition to turbulence will occur and if the turbulent boundary layer re-attaches a so-called laminar separation bubble *(LSB)* will be formed. So far, laminar separation bubbles were primarily a concern for small-aircraft aerodynamics because of their dependence on low to medium Reynolds numbers. However, in-flight measurements published in the 1990's have shown that they affect high-lift devices of commercial transport aircraft in slow flight, as well. This is not too surprising as the Reynolds number for a deployed slat lies in the same range as for the wing of a sailplane, for instance.

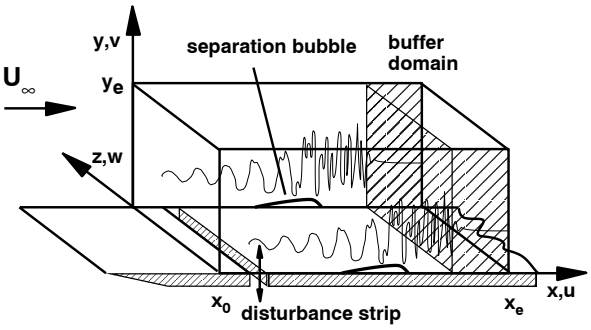

Figure 1: Integration domain for the DNS of a laminar separation bubble.

The present paper will present an overview on recent research on laminar separation bubbles at IAG, University of Stuttgart. The aim of this research was to shed more light on the largely unknown instabilities of transitional laminar separation bubbles and their contribution to laminar-turbulent transition. As a rule, the reader should be aware that "the laminar separation bubble" as a unique or universal feature does not exist. Rather, each bubble depends on the characteristics of the laminar boundary layer, the ensuing pressure gradient, and, not to the least, on the background disturbance level and spectrum of the flow, as will be shown further down. In an attempt to control the influence of the disturbance background as far as possible, most of the present work is based on DNS with carefully selected disturbance combinations with the intention of isolating and understanding different mechanisms.

More recently, experiments in a laminar-flow water channel have been begun and compared with DNS performed in parallel in order to yield a data base for subsequent LES-studies with well-defined inflow conditions.

The present paper consists of three sections. The first of these introduces the numerical method used, the second discusses several key results, such as investigations on the linear (primary) instability of some flows, absolute vs. convective instability, on the influence of disturbance amplitudes on bubble size, on secondary instability, on 3-D disturbance amplification due to oblique breakdown, and on a newly found instability mechanism. The third section is devoted to direct comparisons between water channel experiments and DNS which corroborate part of the present numerical results and the paper ends with conclusions.

Numerical Method

We consider the incompressible flow over a portion of a flat plate with a free-stream pressure gradient specified at the upper boundary of the according integration domain ($y = y_e$ see Fig 1). The coordinate system is chosen such that the coordinate x corresponds to the free-stream flow direction (along the flat plate), y is the direction normal to the plate, and z the spanwise direction. The method described in (Ref 5, 24) and (Ref 18, 23) is used. It is based on a vorticity-velocity formulation of the Navier-Stokes equations, discretised by fourth-order accurate finite differences in x- and y-direction and a Fourier ansatz in z, i.e. periodicity with a prescribed wavelength λ_z is assumed in z. Time integration of the three vorticity transport equations is performed via an explicit Runge-Kutta scheme of fourth-order accuracy.

For the computation of a boundary layer that includes a laminar separation bubble a steady laminar boundary layer is specified at the inflow boundary of the integration domain together with a function $U_p(x)$ at the free-stream boundary. Typically, the latter contains a region of local adverse pressure gradient that causes the laminar boundary layer to separate and to re-attach a short distance further downstream. In such a case, a steady two-dimensional base flow can be computed inde-

pendently from the investigation of disturbances, as in (Ref 24) and (Ref 26). However, for sufficiently large streamwise pressure gradients or high enough Reynolds numbers the flow becomes unsteady and splitting into a steady base flow and an unsteady disturbance flow is no longer possible. But this causes no severe problem since the computations are performed in an unsteady total-flow formulation then.

Wall boundary conditions as in (Ref 24) and outflow conditions which contain the buffer domain of (Ref 12) complement the specification of the problem. The boundary conditions at the wall include the possibility to introduce disturbances via blowing and suction in a disturbance strip placed upstream of the bubble.

In the present numerical method the v-Poisson equation plays the most significant role for several physical and numerical reasons. Firstly, it is through its free-stream boundary condition ($dV/dy = -dU_p/dx$) that the adverse pressure gradient is imposed on the flow. Secondly, this equation directly reflects the elliptical nature of the incompressible flow, because any velocity fluctuation in the downstream part of the domain can be immediately felt upstream. Thirdly, because its solution needs the largest computational resources compared to all other parts of the numerical scheme. In order to reduce the memory requirements for large-scale computations, it was decided to solve the v-Poisson equation in an iterative manner using a multi-grid procedure on four different grids and several V-cycles for convergence acceleration, cf. (Ref 22).

Results

In the following subsections the influence of the numerical error (residual) on the results will be presented, followed by comparisons of DNS results with linear stability theory (LST), several investigations based on LST related to the influence of the wall on the free shear-layer instability and on the possible occurrence of an absolute instability. Then, DNS will show the non-linear influence of the disturbances on the mean flow and compare several mechanisms associated with the question of how can turbulence (which is inherently three-dimensional) arise in a flow that is dominated by two-dimensional instabilities.

The following examples are presented for $Re = U_\infty \cdot L/\nu = 100000$, where L is an arbitrary reference length used for normalisation of the coordinates. For a Blasius boundary layer the x-coordinate can be converted to the Reynolds number based on the displacement thickness δ^* via $Re^* = 1.72077\ \sqrt{x \cdot Re}$. This is always possible at the inflow boundary of the integration domain because all flows start with the Blasius boundary layer at inflow. Further downstream Re^* increases much faster than Blasius due to the displacement effects of the flow with laminar separation bubble. The complete set of parameters for each of the simulations presented in this paper can be found in the according references for each example presented here.

Residual Influence

Compared to earlier investigations with attached boundary layers a much stricter residual (almost machine accuracy) is required for flows with LSBs. This has been demonstrated by Maucher (Ref 15, 27). Figure 2 compares results of two 2-D simulations which differ only in the number of V-cycles used for iterating the v-Poisson equation. In both cases *no* disturbances are introduced via suction and blowing at the wall, i.e. the unsteadiness arises from the initial conditions, numerical residual, numerical round-off, some kind of instability, and possible reflections from the boundaries of the integration domain. Interestingly, the case with larger residual (due to less V-cycles for the solution of the v-Poisson equation) produces a much more regular flow field with a steady point of separation and (the well-known) periodical vortex shedding at re-attachment.

Once the residual is reduced (to its limit) not only the position of the bubble changes, but also the disturbances in its wake. A frequency analysis reveals that the dynamics of the better-converged result is dominated by an unstable frequency band instead of a single frequency as in the first case. So the second realisation is not only better converged but also in better agreement with disturbance amplification according to hydrodynamic instability (based on the Orr-Sommerfeld equation),

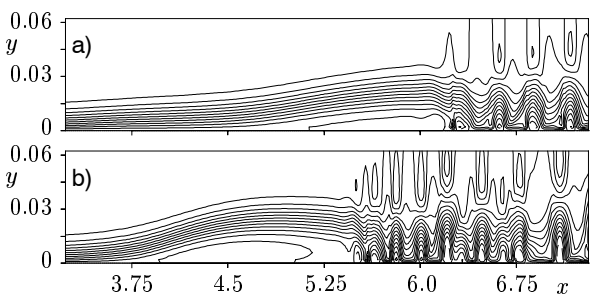

Figure 2: Comparison of instantaneous velocity contours from two simulations with different number of iterations. a) 4 V-cycles; b) 8 V-cycles.

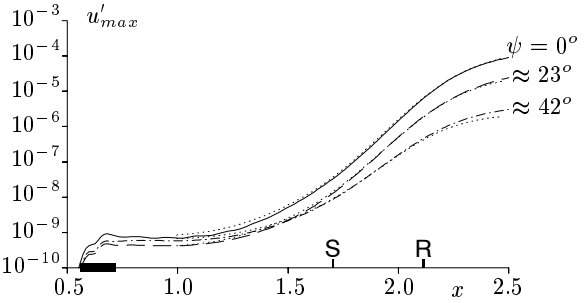

Figure 3: Comparison of u' disturbance maxima with results of linear stability theory ($\cdots$). S = separation; R = re-attachment; ▬ = location of disturbance strip.

because linear stability never predicts a single unstable frequency. This expectation is usually ignored in literature where single-frequency disturbances are more the rule than the exception. A possible explanation for the discrepancy is that selection of a single frequency can occur as a consequence of two effects: upstream feedback of fluctuations by insufficient resolution in a simulation or by reflection of sound from the domain boundaries (or tunnel walls in an experiment), and their amplification by the linear instability of the flow. In light of the present numerical results observations like a "universal Strouhal number" for the high-shear layer instability must be viewed with care.

Primary Instability

Our present knowledge of the primary instability of laminar separation bubbles stems mainly from some theoretical investigations based on hypothetical, free shear-layer like base-flow profiles or modifications thereof (Ref 2, 4, 8, 9, 20, 21). These have the advantage that the influence of parameter variations can be easily studied. But such profiles do not correspond to an actual flow field that fulfils the Navier-Stokes equations. In addition, a local analysis neglects the streamwise structure of the flow (so-called nonparallel effects). However, in direct quantitative comparisons of DNS results with linear stability theory based on base- or mean-flow profiles of the simulations we have shown that small-amplitude disturbances evolve in an extremely good agreement with linear stability theory despite its approximate manner. This is shown in Fig 3 where the normal-to-the wall maxima of the streamwise velocity fluctuation u' for Tollmien-Schlichting waves with different propagation angle relative to the base flow are displayed. In contrast to Fig 2 the present flow is much closer to the leading edge of the flat plate such that Reynolds number and pressure gradient are not large enough to cause a similar unsteadiness. A more complete description of this case can be found in (Ref 25) and (Ref 26), for instance.

These results also show that the disturbance growth with downstream coordinate x increases in a very gradual way already well upstream of the separation point (S). In consequence, there is no reason to distinguish between a free shear layer or 'Kelvin-Helmholtz' instability and the TS-instability of a boundary layer.

Influence of the Wall

A quantitative investigation of the influence of the wall on linear stability theory results has been performed (Ref 23, 26). Figure 4 illustrates the findings of that research for two different wall distances of the "free shear layer". The dashed curves correspond to a boundary layer profile taken from the previous example at $x = 2.0$, where the separation bubble exhibits the strongest reverse flow. This profile was then modified, first by a small shift in u-direction by the amount of maximal reverse flow in order to make that zero (curve (1)), then by different shifts away from the wall, padded with zero velocity (curve (2)). In any

case, a viscid investigation was performed for finite Reynolds number. The results for the largest wall distance in Fig 4 (b) and (d) agree extremely well with the spatial instability of an inviscid shear layer, cf. (Ref 19, Fig 2)). Only for the smallest frequencies, there is an influence of the wall that can be seen in the difference of the phase speed from the theoretical value of 1. The instability and the eigenfunctions of the profile extracted from the DNS-bubble are really far away from the inviscid free shear-layer instability.

As already shown, the shift-over from boundary-layer instability to free shear-layer instability is a very smooth process. This leads to a characteristic evolution of the eigenfunctions of the disturbances: for a boundary-layer TS-wave the disturbance maximum is close to the wall followed by a phase jump, a second maximum, and exponential decay further away, while for a free shear-layer mode there is a maximum exactly at the inflection point of the base-flow profile followed by a sharp phase jump towards the low speed side of the flow and exponential decay in both directions after a certain distance from the high-shear region. Therefore, the profiles in the changeover region which are characteristic for LSBs have three distinct maxima. For practical purposes their relative magnitude can be used to assess the amount of contribution of the free shear-layer instability to the TS-instability: a large shear-layer maximum would indicate more contribution of the shear-layer instability, and vice versa. Since the wall distance of the separated shear layer in a pressure-induced laminar separation bubble (in contrast to a laminar separation bubble found behind a step) increases steadily the initial instability is of TS-type in any case. Only for very large bubbles (and hence shortly before transition) a contribution from a free shear-layer type of instability can be expected.

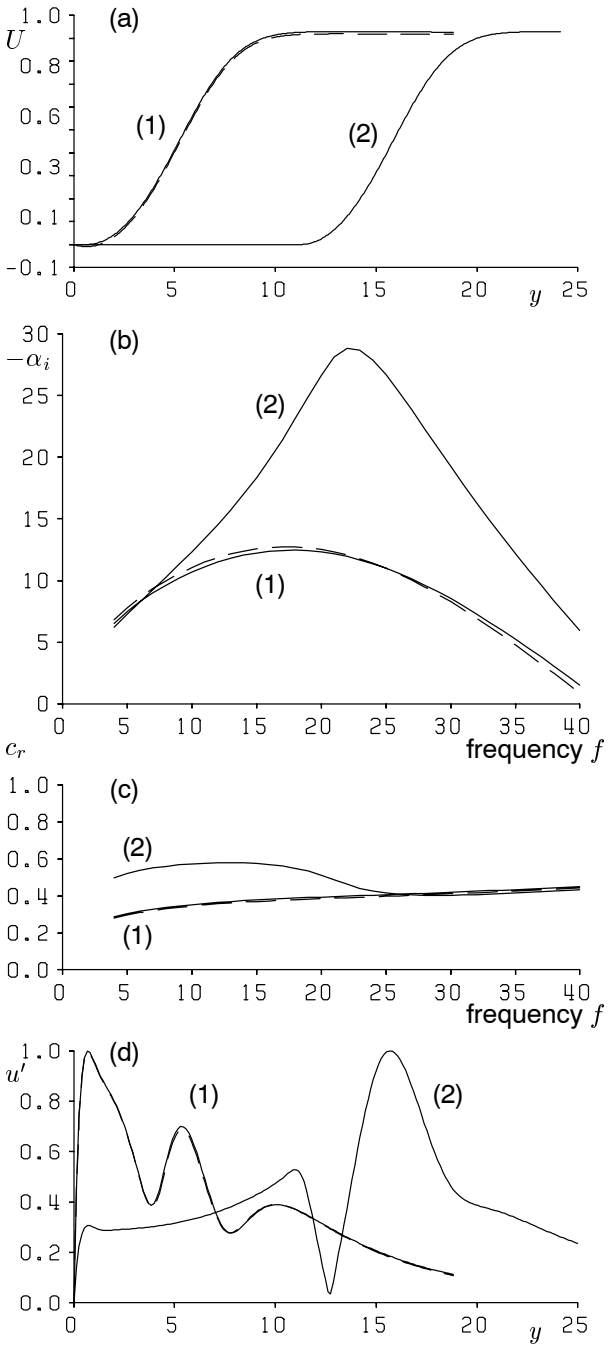

Figure 4: Investigations on the influence of the wall on the instability of the separated shear layer. Note: the y coordinate is stretched by $\sqrt{Re}$, $Re = 100000$. a) base flow; b) amplification rates α_i; c) phase velocities; d) eigenfunctions for the frequency $f = 2\pi f[Hz]\, L/U_\infty = 20$.

Absolute vs. Convective Instability

A long-standing question among many researchers has been the issue whether transition in a laminar separation bubble occurs due to an absolute instability of the flow. Several authors (Ref 1, 2, 8, 9) have shown that a 2-D absolute instability can only be expected once the base flow exhibits 15% reverse-flow intensity in the bubble.

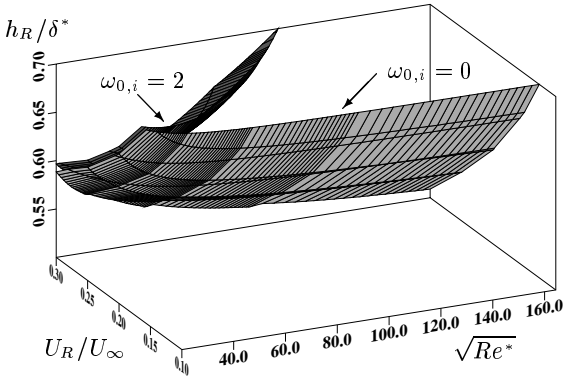

Figure 5: Iso-surfaces of constant temporal amplification.

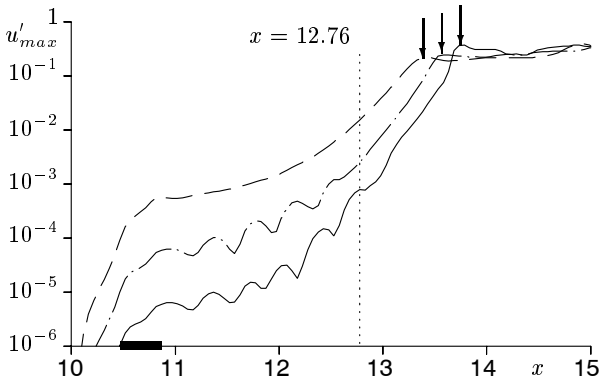

Figure 6: Comparison of disturbance amplitudes for different forcing at the wall: $A_v = 10^{-4}, 10^{-5}, 10^{-6}$ (top to bottom). S = separation; R = re-attachment; ▬ = location of disturbance strip.

Maucher (Ref 15, 27) has tried to refine the boundary between absolute and convective instability by considering two additional parameters, Reynolds number and the (nondimensional) height of the reverse-flow zone. His results are summarized in Fig 5 which shows iso-surfaces of the temporal amplification rate found by a shooting method for complex spatial wavenumber and complex frequency. Here $\omega_{0,i}$ stands for the temporal amplification rate of eigenvalues with zero group velocity. Growth occurs for $\omega_{0,i} > 0$, i.e., above the surface $\omega_{0,i} = 0$, the reverse-flow intensity increases from front to back and its thickness from bottom to top. Because the solutions correspond to zero group velocity there is a true chance for temporal growth according to Gaster (Ref 7) without checking for a pinching of eigenvalues (which is not possible using a shooting method that yields only one eigenvalue at a time).

The present results indicate that time-growing disturbances can be met not only when the intensity of reverse flow is increased beyond 15% but also when the thickness of the reverse-flow zone exceeds $h_R/\delta^* = 0.5$. A weak Reynolds number influence is also observed. Meanwhile, the above theoretical predictions have been validated by comparisons with two DNS, one in (Ref 27), the other unpublished.

Influence of Disturbance Amplitude on Bubble Size

In a LSB instability and base flow are coupled much closer than in an attached boundary layer. Due to large amplification rates and various instabilities, disturbances can reach a non-linear regime within the bubble even if their initial amplitude is 'negligibly' small. Once they are large enough they impose changes on the mean flow in a non-linear manner (that is difficult to predict). Changes of the mean flow can alter the instability and hence the growth of disturbances that follow. An example for such a case where the laminar separation bubble exhibits a low-frequency change of its stability characteristics is described in (Ref 15) and (Ref 27).

Here we consider a simulation with large Re^* at inflow and hence much larger Re^* at separation ($Re^* = 1722$ and 2700, respectively). Upstream forcing is applied with $f = 5$ and three different disturbance amplitudes for the wall-normal velocity component: $A_v = 10^{-4}$, 10^{-5}, and 10^{-6}. The according maxima of u' are shown in Fig 6 and the points of nonlinear saturation of each case are marked by three arrows that touch the respective curve. The results are as expected: for larger forcing transition (in the present simulations, the point of non-linear saturation of the disturbances) occurs further upstream than for small disturbance amplitudes. Since earlier transition means earlier re-attachment, it can be expected that the bubble becomes shorter from its rearward end, a fact that is actually observed in the streamline plots of Fig 7.

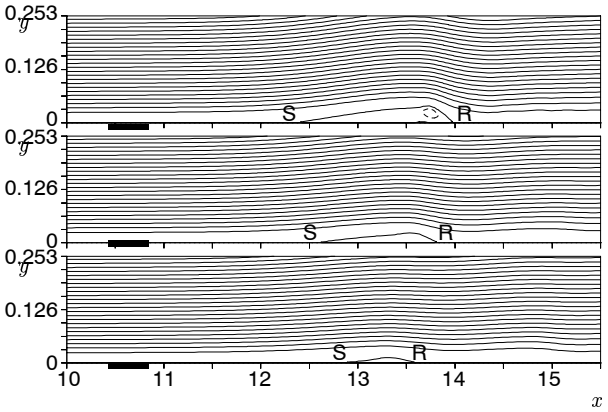

Figure 7: Mean-flow streamlines for simulations with three different forcing amplitudes: $A_v = 10^{-6}, 10^{-5}, 10^{-4}$ (from top to bottom). S = separation; R = re-attachment; ▬ = location of disturbance strip.

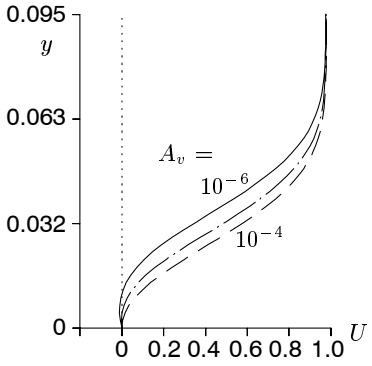

Figure 8: Comparison of mean-flow profiles at $x = 12.76$ for different forcing at the wall.

However, this is not the only effect of the disturbances, since the separation point moves downstream an equally large distance at the same time. A further remarkable effect is that the mean-flow profiles (Fig 8) exhibit a rather unexpected strong dependence on the disturbance amplitudes, as well. Thus, the difference between two profiles is orders of magnitude larger than the local disturbance amplitude (compare Fig 6 and Fig 8). A very similar effect has also been discovered in wind-tunnel experiments by Dovgal *et al.* (Ref 4).

Further analysis of the DNS data has shown that this coupling of transition, reattachment, and separation is related to subtle changes in the streamwise pressure gradient along the wall. In a pressure-induced separation bubble, (S) is not fixed by some surface irregularity and hence highly sensitive to small changes in pressure. Thus, it turns out that a pressure-induced LSB is very sensitive to background disturbances and that these should be taken into account when comparing simulation results with experiments. This is why we have started the work described in the third section in a controlled environment by carefully validating the initial disturbance spectrum.

Secondary Instability

In a two-dimensional boundary layer, three-dimensional disturbances become strongly amplified by a parametric resonance once two-dimensional primary disturbances have attained sufficiently large amplitudes (Ref 10). Typically, this kind of secondary instability amplifies disturbances with subharmonic or fundamental frequency with respect to the two-dimensional one, and its amplification rates are characteristically one order of magnitude larger than that provided by primary instability. Due to non-linear interactions the wavenumber-frequency spectrum fills up very rapidly which indicates a breakdown of the flow into small-scale unsteady structures. For many laminar separation bubbles, however, our simulations show that such an instability is only marginally relevant because it is restricted to a very narrow streamwise region.

One typical result taken from (Ref 23, 25, 26) is illustrated in Fig 9 for a case where a fundamental two-dimensional disturbance with $u'_{max} \approx 10^{-5}, f = 18$ is forced at $x \approx 0.65$ together with a subharmonic ($f = 9$) three-dimensional one at $u'_{max} \approx 10^{-9}$. For comparison, results of primary instability (LST) and of secondary instability theory (SST) are also included (with their initial amplitudes adjusted to the DNS). Due to the presence of the laminar separation bubble, the amplification rate for the primary instability is now one order of magnitude larger than in a Blasius boundary layer and an additional amplification of 3-D disturbances

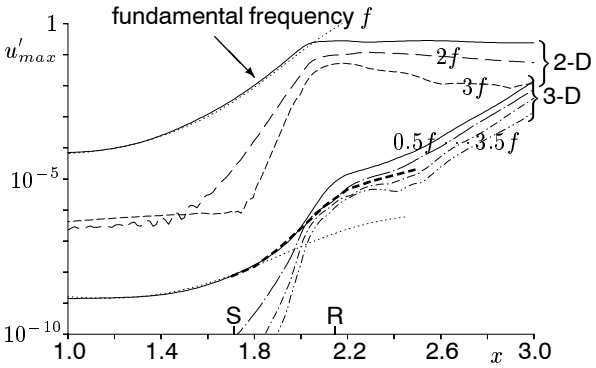

Figure 9: Amplification curves u'_{max} of two- and three-dimensional disturbance components for the case with subharmonic resonance. Comparison with LST ($\cdots$) and SST (**- - -**). S = separation; R = re-attachment.

due to secondary instability that starts around $x = 1.8$ as the 2-D disturbance passes 1% is not as dramatic as might be expected. In addition, once the 2-D disturbance saturates at $u' \approx 20\%$ the secondary amplification is greatly reduced such that, for the present scenario, the 3-D disturbances do not reach a saturation level within the integration domain. Flow visualisations have shown that the 3-D disturbances of the SST get destroyed by the 2-D ones in the saturated regime: 3-D vorticity is redistributed and convected away by the large-amplitude 2-D rollers that develop downstream of the bubble. The higher harmonic wave components which are also included in Fig 9 confirm this process by their large amplitudes. In fact, large-amplitude 2-D forcing can control the flow by delaying transition, a detail that has independently been observed in experiments by Dovgal et al., for instance.

Here, a subharmonic scenario (that would lead to so-called H-type transition in a Blasius boundary layer) has been studied. But similar investigations have been performed for fundamental resonance (K-type) and mixed scenarios, for the base flow considered here, as well as for the one presented in Fig 7 (Ref 23, 26).

Oblique Breakdown

As an alternative to classical secondary instability scenarios, a mechanism which was first discovered for transonic flow and termed “oblique transition”, because of its dependence on the non-linear interaction of oblique waves, was investigated as well.

Figure 10 depicts the evolution of the spectral amplitudes of this case in the same base flow as before. Throughout the paper, the first index for a frequency-spanwise-wavenumber mode means multiples of the fundamental frequency and the second multiples of the basic spanwise wavenumber $\gamma = 2\pi/\lambda_z$. Now, the primary disturbance (identified as mode (1, $pm1$) consists of a pair of oblique Tollmien-Schlichting waves ($f = 18$) with an initial angle of $\psi \approx 28^o$ relative to the x-axis and an initial amplitude $u'_{max} \approx 10^{-4}$. Clearly, the dominant mode follows linear stability theory rather closely. All other modes arise due to non-linearity which leads to a rapid fill-up of the spectrum at $x \approx 2.0$. Since the largest of the non-linearly generated modes is mode (0,2) the re-attachment, as well as the ensuing boundary layer, exhibit longitudinal streaks in the temporal mean. Occasionally, such streaks have already been observed in experiments, e.g. (Ref 3). Inger has tried to relate them to a Görtler instability (Ref 11). However, for the present case it is clear that they arise from transition, since they are an inherent property of the so-called “oblique breakdown” scenario.

Further studies of this kind of mechanism showed that the optimal growth of the streak modes appears when oblique waves with an obliqueness angle of $\psi \approx 20^o$ are forced. This occurs because the growth of the primary modes due to LST is reduced for larger angles and because no oblique breakdown is possible for $\psi \to 0$.

A direct comparison of instantaneous vorticity contours from the (hindered) subharmonic scenario in Fig 9 with those from Fig 10 is shown in Fig 11. This illustrates the interpretation given above, that the flow is controlled by spanwise oriented ‘rollers’ in the first case, and that a rapid breakdown into small-scale structures appears in the second. Such small-scale 3-D structures are necessary for the rapid development of a turbulent boundary

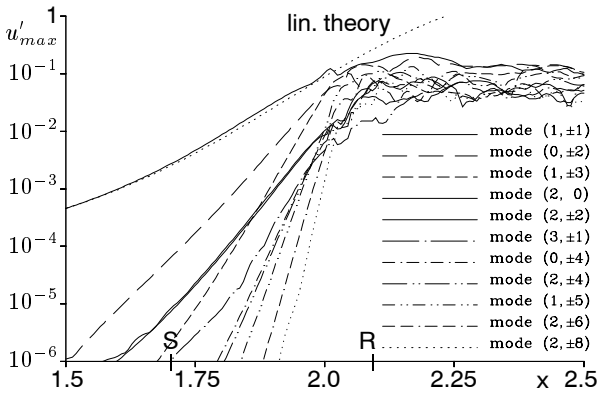

Figure 10: Amplification of individual spectral modes for large 3-D disturbance amplitude.

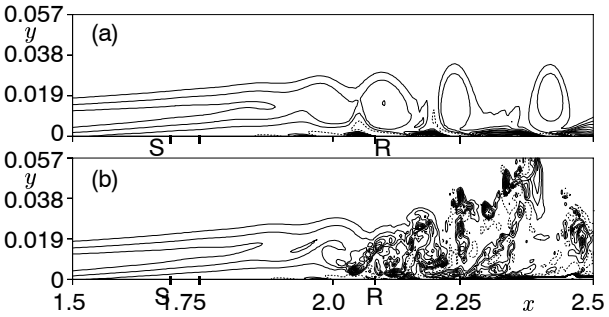

Figure 11: Comparison of instantaneous vorticity contours for subharmonic resonance (a) and "oblique breakdown" (b).

layer in a laminar separation bubble. Thus, it appears that the mechanism studied here can be relevant for production of turbulence in a LSB. This has also been verified in mixed secondary-oblique scenarios in (Ref 25).

A New Type of Instability

When the Reynolds number at separation is increased, a new kind of secondary instability mechanism is observed which leads to *temporal* amplification of small-scale three-dimensional disturbances that are trapped in the separation bubble. More information on this case can be found in (Ref 15) and (Ref 17). In contrast to above Re^* at separation is now approx. 2400 instead of 1250.

Figure 12 displays amplitudes of selected modes

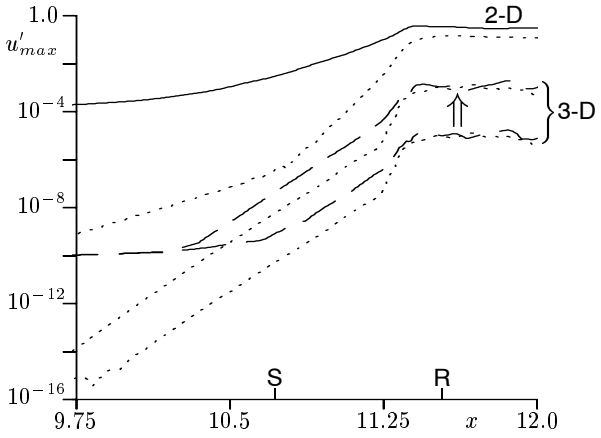

Figure 12: Disturbance amplitudes of 2-D (solid) and 3-D (dashed) waves in the vicinity of the bubble. Dotted lines: higher harmonics; arrow: 3-D temporal growth; S - separation, R - re-attachment.

for two time intervals. A large-amplitude 2-D TS-wave has been forced at $x \approx 8$ together with very small 3-D disturbances. Since the 2-D disturbances are periodic they do not differ for a later time compared to the earlier one. This is in clear contrast to the 3-D disturbances which are two orders of magnitude larger for the second time interval shown in the figure. An arrow is used to highlight the temporal growth of the 3-D disturbances.

It turned out that permanent forcing of the 3-D disturbances is not necessary because a one-instant 3-D time impulse at the wall is sufficient to initiate the growth. A quantification of the temporal growth initiated by a short-time pulse leads to the results presented in Fig 13, where the dependence of the temporal growth rate ω_i on the spanwise wave number is shown. It turns out that regions of subharmonic and fundamental disturbance amplification alternate with spanwise wave number. This indicates that the mechanism found is somehow related to the secondary instability discovered by Herbert (Ref 10).

More investigations with an additional buffer domain applied in the upstream part of the integration domain and for the 3-D modes only indicated that the responsible area for amplification is the reattachment region. By comparing the development of the 3-D disturbances with the dynamics of the 2-D high-shear layer Maucher et al. (Ref 16, 17)

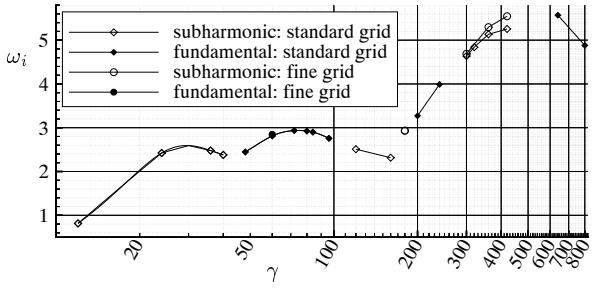

Figure 13: Secondary temporal amplification rate ω_i versus spanwise wave number $\gamma = 2\pi/\lambda_z$ for different discretisations.

identified the reason for the instability as the entrainment of three-dimensionality by the upstream motion in the laminar separation bubble that includes an uplift of 3-D motion into the initially two-dimensional shear layer. Since this process is repeated periodically, the 3-D amplitudes can grow from cycle to cycle until they reach a level with non-linear saturation. Once this level is reached, the process just described is still operative in order to destroy the 2-D shear layer repeatedly. This is visualised by iso-surfaces of spanwise vorticity in Fig 14. The dynamics of this kind of laminar separation bubble transition resembles the breaking of waves which approach a shore line.

An interesting aspect of the scenario shown is that it is very efficient for small obliqueness angles of the involved primary disturbances, i.e. it is not restricted to a strictly two-dimensional disturbance. Interestingly, weakly oblique disturbances have been already observed in several free-flight measurements of the natural disturbance spectra in airfoil boundary layers.

Comparisons with Experiments

Systematic experiments on laminar separation bubbles have been performed by (Ref 4, 6, 28, 29), and others. Typically, when comparing simulations (RANS, LES, DNS) with experiments some 'typical' mean-flow characteristics, like the position of separation, transition, re-attachment, or the length of the bubble are used to validate the computations. However, in light of the results presented in the previous sections, one should be warned, not to neglect the influence of the disturbance spectrum, regardless of its smallness!

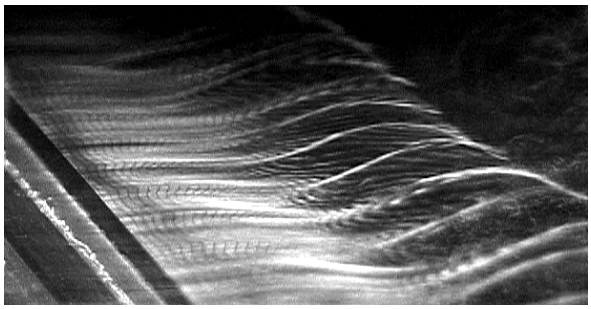

Figure 15: Experimental hydrogen-bubble visualisation of the high-shear layer in a laminar separation bubble undergoing transition.

The laminar water tunnel at IAG was especially designed to study transition in Blasius boundary layers and in separation bubbles. Because of the large scales in water, this water tunnel is particularly suitable for flow visualization, as well. A at first negative, then positive streamwise pressure gradient is imposed on a flat-plate boundary layer (that would otherwise correspond to the Blasius boundary layer) by a displacement body mounted opposite to the plate, such that a laminar separation bubble is obtained in the decelerated region. The experimental set-up and the non-intrusive quantitative measurements (using a Laser-Doppler anemometer, LDA and Particle-Image Velocimetry, PIV) are described in more detail in (Ref 13, 14). Already before performing a lot of quantitative measurements it was possible to find qualitative confirmation of the DNS results of Maucher by means of flow visualisations. Features like the spanwise waviness of the oscillating shear layer shown in Fig 15, as well as its breakdown compare very favourably with numerical observations like the one presented in Fig 14.

Additional DNS have been made parallel to the experimental measurements with base-flow parameters and boundary conditions closely matched to the experiments. The velocity profile at the inflow boundary, for instance, was obtained from a preceding 2-D DNS of a strongly accelerated boundary layer (starting from a Blasius solution well upstream of the displacement body in the experiment) with the favourable pressure gradient chosen to match the experimental values up to the narrowest section, since the measured profile

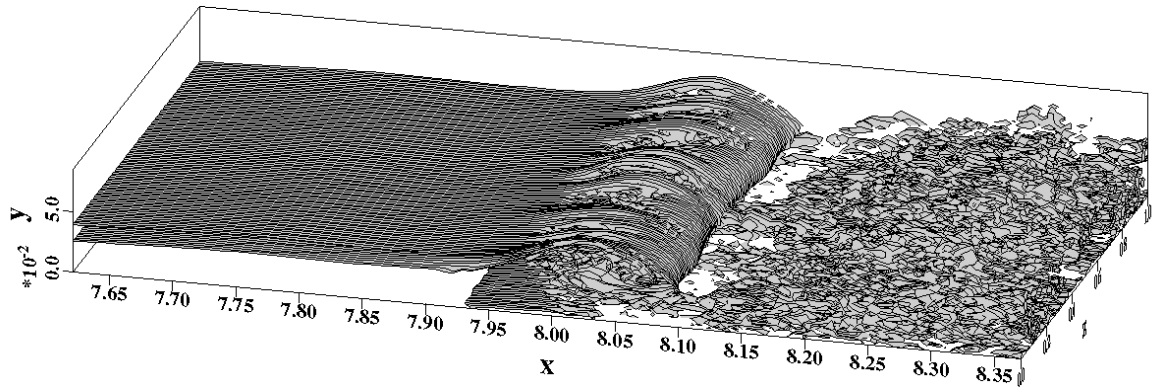

Figure 14: Breakdown of the free shear layer into fine-scale turbulence. Iso-surfaces of the spanwise vorticity. Note: The coordinates in this figure should be multiplied by 1.5 in order to make the normalisation consistent with the other figures.

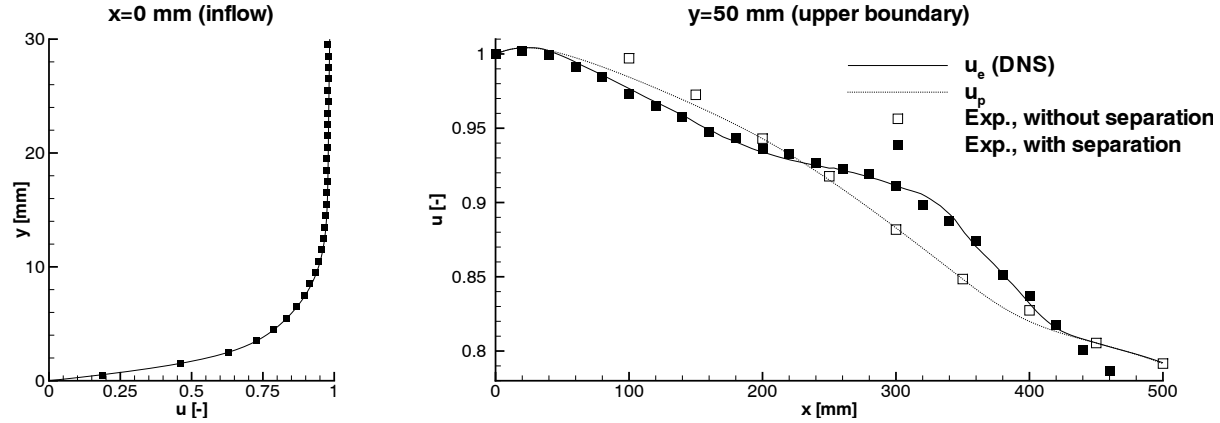

Figure 16: Streamwise mean velocity at $x = 0\ mm$ (left) and $y = 50\ mm$ (right). DNS results u_e (solid line), potential velocity U_p prescribed in DNS (dotted line); Measurements with (filled symbols) and without separation (open symbols).

could not be represented by an analytical (Falkner-Skan) solution ($H_{12} \approx 1.6$ at the inflow). As can be seen in Fig 16, the u-velocity profile from measurements and computations at $x = 0\ mm$ turned out to be in excellent agreement. At the free-stream boundary the potential velocity distribution U_p is chosen according to measurements where separation was suppressed by artificially causing transition prior to the laminar separation point (Fig 16). It serves as initial condition at the free-stream boundary in the DNS and finally the mean edge-velocity distribution u_e almost matches the experimental measurements with separation bubble. Since this velocity condition at the upper boundary is not fixed, but rather comes out of the boundary-layer interaction model, it can already be considered a result of the DNS. Good agreement of DNS data with experiments (Fig 16) therefore gives a first proof of the comparability of the separation bubbles observed in the experiment and in the DNS. Furthermore, it should be emphasized that the actual velocity prescribed at the upper boundary is unsteady and the results presented in the diagram are time-averaged.

A two-dimensional TS-wave and a steady three-dimensional modulation are forced by means of the classical vibrating ribbon technique and spanwise spacers on the plate surface.Comparisons with an undisturbed (experimental) flow indicate that the features of the forced flow are very similar to the “natural case”. The main differences are slight amplitude variations of the shear-layer oscillations, some irregularity regarding the preferred spanwise wave length of the transitional structures, and the length of the bubble (which is shorter for lower disturbance amplitude, in agreement with the numerical results presented above). Only based on periodical forcing it was possible to trace the complete flow-field using phase-locked LDA. For comparisons with DNS and linear stability theory (LST) the LDA measurement results have been Fourier analysed in time and spanwise direction with respect to the frequency of the wire ($f = 1.1\ Hz$, $U_\infty = 0.125\ m/s$) and the spanwise wavenumber according to $\lambda_z = 58\ mm$.

The dominant initial disturbance is the 2-D Tollmien-Schlichting wave forced by the ribbon. Its downstream development (amplification) is compared with DNS and LST in Fig 17. In the experiment the TS-wave could only be detected after it grew to $u'_{max} > 2 \cdot 10^{-3}$. Then, experimental and numerical results perfectly match from $x = 230\ mm$ onwards even shortly beyond saturation. Good agreement with LST confirms the primary convective nature of the disturbance. Calculation and experiment also predict the same amplitude, growth rate and saturation level for the non-linearly generated higher harmonic disturbance (2,0).

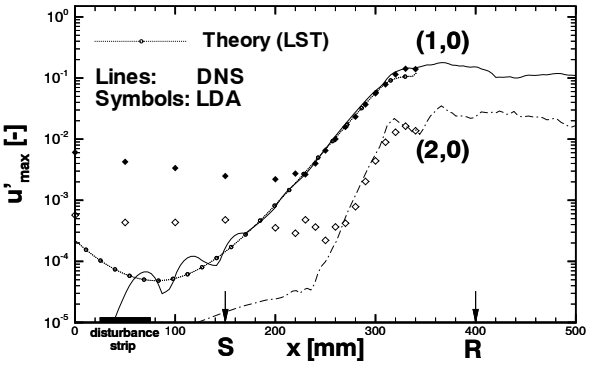

Figure 17: Amplitude development of the maximum 2-D streamwise velocity fluctuations u'_{max}.

Unfortunately, the initial disturbance spectrum in the experiment is not yet completely understood. It consists of several extra modes (presumably from some transient growth mechanism) which slowly decay with x, as can be seen in Fig 17 at $x < 230\ mm$. Also, the largest 3-D disturbance corresponds to mode (0,2) instead of (0,1) which would exactly match the wavelength introduced by the spacers. Comparisons with 3-D DNS have shown that this mode is involved in the transition process because it helps to generate the unsteady 3-D modes (1, $\pm$2) by interaction with the 2-D TS-wave (1,0). This explains the quasi-perfect agreement of the spatial amplification rates between simulation and experiment in Fig 18 once mode (0,2) is included in the simulation. Omitting this disturbance in the simulation led to another scenario.

Conclusions

Several basic mechanisms related to instability and transition in laminar separation bubbles have been isolated and studied. As far as possible, the present DNS results have been verified by com-

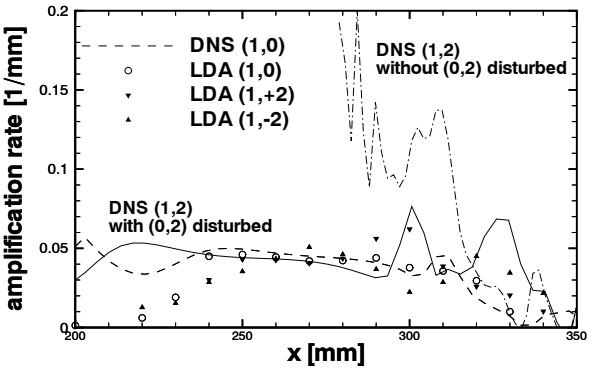

Figure 18: Amplification rates of the maximum 3-D streamwise velocity fluctuations u'_{max}.

parisons with LST, experiments and grid refinement studies. Thus, it turned out that extreme care must be taken to reduce background disturbances as far as possible when trying to identify the mechanisms at hand. Also, the overall size of the bubble appeared to be very sensitive to small-amplitude disturbances and its mean-flow parameters exhibit large variations which would become unpredictable if the disturbance amplitudes were not known. The border between absolute and convective instability was revisited and further refined in terms of Reynolds number and thickness of the reverse-flow zone. Secondary instability and oblique breakdown were compared with the aim to identify the most relevant mechanism for amplification of three-dimensional disturbances. For large Reynolds numbers a new kind of secondary instability was found which leads to temporal growth of 3-D disturbances on the basis of a large-amplitude shear layer oscillation, regardless whether this is produced by an exactly 2-D TS-wave or by weakly oblique waves. Comparisons with ongoing experiments indicate good agreement of the unsteady disturbance development, once the initial amplitudes have been found. Note: these latter cannot be measured directly due to their small initial amplitudes.

References

[1] Alam, M., Sandham, N.D. (2000), Direct numerical simulation of 'short' laminar separation bubbles with turbulent reattachment, J. Fluid Mech. 410, May 2000, pp. 1-28

[2] Allen, T., Riley, N. (1995), Absolute and convective instabilities in separation bubbles, Aeron. J. Royal Aeron. Soc., Dec. 1995, 439-448.

[3] Althaus, D. (1981), Drag measurements on airfoils, XVII OSTIV-Kongress, Paderborn.

[4] Dovgal, A.V., Kozlov, V.V., Michalke, A. (1994), Laminar boundary layer separation: Instability and associated phenomena, Progr. Aerospace Sci. 30, 61-94.

[5] Fasel, H., Rist, U., Konzelmann, U. (1990), Numerical investigation of the three-dimensional development in boundary layer transition, AIAA J. 28 (1), 29-37.

[6] Gaster, M. (1966), The structure and behaviour of laminar separation bubbles, AGARD CP-4, Flow separation, part II, 813-854.

[7] Gaster, M. (1968), Growth of disturbances in both space and time, Phys. Fluids 11 (4), 723-727.

[8] Gaster, M. (1991), Stability of velocity profiles with reverse flow, in: M.Y. Hussaini, A. Kumar, C.L. Streett (Eds.), Instability, Transition and Turbulence, ICASE-Workshop, Berlin, Springer, 212-215.

[9] Hammond, D.A., Redekopp, L.G (1998), Local and global instability properties of separation bubbles, Eur. J. Mech. B/Fluids 17 (2), 145-164.

[10] Herbert, Th. (1988), Secondary instability of boundary layers, Ann. Rev. Fluid Mech. 20, 487-526.

[11] Inger, G.R. (1986), A theoretical study of spanwise-periodic 3D disturbances in the wake of a slightly stalled wing at low Reynolds numbers, Aerodynamics at Low Reynolds numbers $10^4 < Re < 10^6$, Royal Aeronautical Society, London, Oct. 1986.

[12] Kloker, M., Konzelmann, U., Fasel, H. (1993), Outflow boundary conditions for spatial Navier-Stokes simulations of transitional boundary layers, AIAA J. 31 (4), 620-628.

[13] Lang, M., Marxen, O., Rist, U., Wagner, S. (2001), Experimental and numerical investigations on transition in a laminar separation bubble, in: S. Wagner, U. Rist, H.J. Heinemann, R. Hilbig (Eds.), New Results in Numerical and Experimental Fluid Mechanics III, Proc. 12. DGLR-Fachsymposium AG STAB, Stuttgart, 15.-17.11.2000, NNFM Vol. 77, Springer-Verlag, 194-201.

[14] Lang, M., Rist, U., Wagner, S. (2002), Investigation on disturbance amplification in a laminar separation bubble by means of LDA and PIV, Proc. 11th Int. Symp. Appl. Laser Tech. Fluid Mech., 8.-11. July, Lisbon, Portugal.

[15] Maucher, U. (2001), Numerische Untersuchungen zur Transition in der laminaren Ablöseblase einer Tragflügelgrenzschicht, Dissertation Universität Stuttgart.

[16] Maucher, U., Rist, U., Kloker, M., Wagner, S. (2000), DNS of laminar-turbulent transition in separation bubbles, in: Krause, E., Jäger, W. (Eds.), High Performance Computing in Science and Engineering '99, Springer-Verlag, Berlin, Heidelberg, pp. 279-294.

[17] Maucher, U., Rist, U., Wagner, S. (1999), Transitional structures in a laminar separation bubble, in: W. Nitsche, H.J. Heinemann, R. Hilbig (Eds.), New Results in Numerical and Experimental Fluid Mechanics II, NNFM Vol. 72, Vieweg, 307-314.

[18] Maucher, U., Rist, U., Wagner, S (2000)., A refined interaction method for DNS of transition in separation bubbles, AIAA Journal Vol. 38, No. 8, Aug. 2000, 1385-1393.

[19] Michalke, A. (1965), On spatially growing disturbances in an inviscid shear layer, J. Fluid Mech. 23, 521-544.

[20] Michalke, A. (1990), On the inviscid instability of wall-bounded velocity profiles close to separation, ZFW 14, 24-31.

[21] Michalke, A., Kozlov V.V., Dovgal A.V. (1995), Contribution to the instability of laminar separating flows along axisymmetric bodies. Part I: Theory, Eur. J. Mech. B/Fluids 14 (3), 333-350.

[22] Rist, U. (1991), An accurate and efficient code for the direct numerical simulation of transition to turbulence, in: M. Durand and F. El Dabaghi (Eds.), Proc. High-Performance Computing II, Montpellier, France, North-Holland, Amsterdam, 467-478.

[23] Rist, U. (1999), Zur Instabilität und Transition in laminaren Ablöseblasen, Habilitation Universität Stuttgart, Shaker, Aachen, Maastricht, 1999.

[24] Rist, U., Fasel, H. (1995), Direct numerical simulation of controlled transition in a flat-plate boundary layer, J. Fluid Mech. 298, 211-248.

[25] Rist, U., Maucher, U. (1994), Direct numerical simulation of 2D and 3D instability waves in a laminar separation bubble, AGARD CP-551, Application of Direct and Large Eddy Simulation to Transition and Turbulence, Chania, Crete, 34-1 – 34-7.

[26] Rist, U., Maucher, U., Wagner, S. (1996), Direct numerical simulation of some fundamental problems related to transition in laminar separation bubbles, in: J.-A. Désidéri, C. Hirsch, P. Le Tallec, M. Pandolfi, J. Périaux (Eds.), Computational Fluid Dynamics '96, John Wiley & Sons, Ltd., 319-325.

[27] Rist, U. Maucher, U. (2002), Investigations of time-growing instabilities in laminar separation bubbles, submitted to: European Journal of Mechanics B/Fluids, December 2001.

[28] Watmuff, J.H. (1999), Evolution of a wave packet into vortex loops in a laminar separation bubble, J. Fluid Mech. 397, 119-169.

[29] Würz, W. (1996), Experimental investigations of transition development in attached boundary layers and laminar separation bubbles, in: H. Körner, R. Hilbig (Eds.), New Results in Numerical and Experimental Fluid Mechanics, 10. AG STAB/DGLR Symposium, NNFM 60, Braunschweig: Vieweg, 1997, 413-420.